

# Spin-dependent transition rates through exchange coupled localized spin pairs during coherent spin excitation

A. Gliesche<sup>a,b</sup>, C. Michel<sup>a,c</sup>, V. Rajevac<sup>d</sup>, K. Lips<sup>d</sup>, S.D. Baranovskii<sup>c</sup>, F. Gebhard<sup>c</sup> and C. Boehme<sup>a</sup> \*

<sup>a</sup>University of Utah, Physics Department, 115S 1400E, Salt Lake City, Utah 84112, USA

<sup>b</sup>Institut de théorie des phénomènes physiques, Ecole Polytechnique Fédérale, CH-1015 EPF-Lausanne, Switzerland

<sup>c</sup>Department of Physics and Material Sciences Center,

Philipps-University, Renthof 5, D-35032 Marburg, Germany and

<sup>d</sup>Hahn-Meitner-Institut Berlin, Kekuléstr. 5, D-12489 Berlin, Germany

(Dated: November 9, 2021)

The effect of exchange interactions within spin pairs on spin-dependent transport and recombination rates through localized states in semiconductors during coherent electron spin resonant excitation is studied theoretically. It is shown that for identical spin systems, significant quantitative differences are to be expected between the results of pEDMR/pODMR experiments where permutation symmetry is the observable as compared to pESR experiments with polarization as the observable. It is predicted that beat oscillations of the spin nutations and not the nutations themselves dominate the transport or recombination rates when the exchange coupling strength or the field strength of the exciting radiation exceed the difference of the Zeeman energies within the spin pair. Furthermore, while the intensities of the rate oscillations decrease with increasing exchange within the spin pairs, the singlet and triplet signals retain their relative strength. This means that pEDMR and pODMR experiments could allow better experimental access to ESR forbidden singlet transitions which are hardly or not at all accessible with conventional pulsed electron spin resonance spectroscopy.

PACS numbers: 76.30.-v 76.70.Hb 76.90.+d 72.20.-i

Keywords: magnetic resonance; spin-dependent processes; Rabi frequency, exchange coupling

## I. INTRODUCTION

In recent years, pulsed electrically and optically detected magnetic resonance methods (pEDMR and pODMR, respectively) have attracted increasing attention due to their higher sensitivity in comparison to the conventional pulsed electron spin resonance (pESR) technique. While pODMR has been applied to the investigation of molecular excited states and radical pair analysis for more than 30 years<sup>1,2,3,4</sup>, pEDMR studies have been reported only recently when different electrical detection schemes for spin coherence became available allowing the observation of pulsed electron<sup>5,6</sup> and even nuclear spin resonances<sup>7</sup>. For any pODMR and pEDMR experiment there must be a spin-dependent electronic mechanism which encodes spin-information into electronic transitions which are then detected either by means of their radiative emissions (with pODMR) or through charging and recombination (with pEDMR). The latter has been studied in the recent past in particular to find potential spin to charge-conversion mechanisms for the electric readout in solid state based spin quantum computers<sup>5,8</sup>.

PODMR and pEDMR are typically performed as transient nutation style experiments which means the evolution of the electronic transition rates during coherent excitations are recorded by measurement of the relaxation of the respective observable after the excitation as a function of the excitation length  $\tau$ . This allows the ob-

servation of Rabi oscillation<sup>2</sup> and also, by application of pulse trains with alternating excitation phases, the observation of rotary echoes<sup>1,5</sup>. The information gained from these experiments are coherence times, dephasing times as well as insights into the coupling between the spin centers involved. For pESR, the behavior of pairs of spin  $s = \frac{1}{2}$  in transient nutation experiments has been established more than a decade ago when theoretical studies described the pair evolution in presence of spin exchange and dipolar coupling<sup>9</sup> and also under the influence of the hyperfine coupling due to the presence of nuclei with non-vanishing spin<sup>10</sup>. These pESR approaches are similar but not completely applicable to pEDMR and pODMR experiments due to the difference of their observables. While the free induction decay of pESR experiments always represents the polarization of a spin ensemble at the end of the spin excitation, pODMR/pEDMR transients reflect the permutation symmetry or antisymmetry of the spin pairs that control the measured electronic transition rates. The consequences of this difference can be drastic as explained in detail in a recent study of spin-dependent transport and recombination through weakly spin coupled pairs<sup>11</sup>. When excitation intensities are increased, the Rabi-nutation frequency observed with pEDMR/pODMR will abruptly double while the nutation observed with pESR will not. This raises the question of whether the different behavior of pairs of spin  $s = \frac{1}{2}$  as observed for weakly exchange coupled spin pairs does also imply that pEDMR/pODMR experiments will differ from the predictions for pESR experiments for strongly exchange coupled pairs which would render the transient nutation literature on radical pairs<sup>9,10</sup> not fully

\*email: boehme@physics.utah.edu

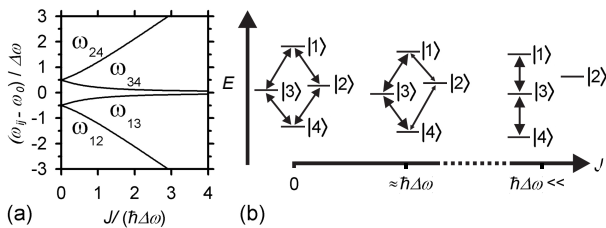


FIG. 1: (a) Plot of the ESR allowed transition frequencies  $\omega_{ij} = \frac{1}{\hbar}(E_i - E_j)$  with  $(ij) \in \{12, 13, 24, 34\}$  as function of  $J$ . Transitions  $\omega_{12}$  and  $\omega_{24}$  involve the state  $|2\rangle$  with high singlet content. For the plot, Larmor frequencies of  $\omega_{a,b} = 10 \pm 0.01$  GHz have been assumed. (b) The energy term scheme and ESR allowed transitions for a spin  $\frac{1}{2}$  pair with presence of weak ( $\Delta\omega \gg \frac{J}{\hbar}$ , left), intermediate ( $\Delta\omega \approx \frac{J}{\hbar}$ , center) and strong ( $\Delta\omega \ll \frac{J}{\hbar}$ , right) exchange coupling. The sketches define the nomenclature of the states and transitions discussed in this study.

applicable. Moreover, for previous studies for the calculation of pESR detected transient nutation<sup>9</sup> experiments, one of the assumptions made was that exchange coupling was smaller than the separation of the Larmor frequencies within the coupled radical pairs. This assumption, which is realistic for many radical pair systems simplified the problem sufficiently enough so that the results could be calculated analytically. In contrast, for charge carrier systems in semiconductors with weak spin-orbital coupling, this assumption does not necessarily always hold and thus, it limits the applicability of these previous studies even further.

In the following, we present a numerical study of transport and recombination through localized exchange coupled spin pairs in semiconductors during coherent spin excitation. The purpose is to elucidate differences between transient nutation experiments on exchange coupled radical pairs detected by pESR in contrast to the detection by pODMR/pEDMR. We focus in particular on the question when the observed spin pairs act as two single spin systems or one two-spin systems which turned out to be one of the key differences for pESR and pEDMR/pODMR detected transient nutation of weakly coupled spin pairs. Another question that is discussed is whether magnetic resonance induced triplet-singlet transitions which become increasingly forbidden with increasing exchange coupling will reduce the observed signal intensities in the same way as for pESR or not. It shall be pointed out here that the focus of this study deals solely with spin-selection rule based electronic transitions between paramagnetic states in weakly spin-orbital coupled systems. Typical examples for this would be charge carrier pairs in semiconductors such as electron-hole pairs, defect pairs such as donor-acceptor pairs or radical pairs in molecular systems or solid state host environments. The study deals with the opposite situation of the pair states discussed in Ref.<sup>11</sup> which described spin pairs of negligible exchange. It shall be emphasized that other

spin to charge conversion mechanisms are known (e.g. the nuclear spin measurement by means of hyperfine coupling to unequally populated quantum Hall edge channels<sup>7</sup>) whose behaviors during pEDMR experiments do not necessarily follow the descriptions given here.

## II. PAIR MODEL

The pair model that we use in this study has been described in detail elsewhere<sup>11,12</sup> and therefore it is described here only briefly. The underlying idea is that spin dependency of electronic transitions comes from the formation of spin  $s = \frac{1}{2}$  pairs consisting of electrons or holes which exist for a short time (intermediate pairs) before they either dissociate or collapse into one doubly occupied electronic state under formation of a singlet state. The probability for this collapse depends on the singlet content of the spin pairs when spin conservation due to sufficiently weak spin-orbit coupling is given. Thus, the spin dynamics that is determined by the spin Hamiltonian of these pairs will ultimately control the electronic transition rates which in turn may determine macroscopic observables such as luminescence or conductivity. Under magnetic resonant conditions, a constant magnetic field  $\vec{B}_0 = B_0 \hat{z}$  and an oscillating magnetic field  $\vec{B}_1 = B_1 (\hat{x} + i\hat{y}) e^{-i\omega t}$  that rotates in a plane perpendicular to the  $B_0$  field, are present. This leads to a Hamiltonian  $\hat{H} = \hat{H}_0 + \hat{H}_J + \hat{H}_1(t)$  of the intermediate spin pairs consisting of the contributions  $\hat{H}_0 = \frac{1}{2}\mu_B B_0 [g_a \hat{\sigma}_z^a + g_b \hat{\sigma}_z^b]$  of the constant magnetic field,  $\hat{H}_1(t) = \frac{1}{2}g\mu_B B_1 [\hat{\sigma}_+^a + \hat{\sigma}_+^b] e^{-i\omega t}$  of the rotating magnetic field and the Heisenberg exchange coupling  $\hat{H}_J = -J \vec{S}_a \vec{S}_b$ . In these terms,  $\mu_B$  represents Bohr's magneton,  $\hat{\sigma}_j^i$  is the Pauli matrix  $j$  of spin  $i$ , (with  $j \in \{\hat{x}, \hat{y}, \hat{z}\}$  and  $i \in \{a, b\}$ ),  $g_i$  and  $\vec{S}_i$  are the Landé-factors and the spin operators of spin  $i$ , respectively while  $g$  represents the vacuum electron Landé factor that is used when the differences between the weakly coupled spin partners are negligible (e.g. for the weak influence of the  $B_1$  field when  $B_1 \ll B_0$ ). Note that in contrast to previous studies on weakly coupled spin pairs<sup>11,13</sup>, the pair Hamiltonian here includes a non-negligible contribution  $\hat{H}_J$  of the exchange within the pairs. It is the investigation of this coupling which is in the focus of this study. The time-independent Hamiltonian  $\hat{H}_0 + \hat{H}_J$  has the eigenvalues

$$E_{1,4}(J) = -\frac{1}{4}J \pm \frac{1}{2}\hbar\omega_0 \quad (1)$$

$$E_{2,3}(J) = \frac{1}{4}J \pm \frac{1}{2}\sqrt{J^2 + \hbar^2\Delta\omega^2}$$

where  $\omega_0 = \omega_a + \omega_b$  and  $\Delta\omega = \omega_a - \omega_b$  are the sum and the difference of the Larmor frequencies  $\omega_{a,b}$  within the pair. As expected for spin  $s = \frac{1}{2}$  pairs, the energy eigenvalues represent a four-level system and, as long as the first order processes are considered only, there

are four allowed transitions as well known from conventional ESR spectroscopy. Fig. 1 shows the transition frequencies of all four transitions as a function of the exchange coupling strength  $J$ . One can see that with increasing exchange, the energies of the  $|1\rangle \leftrightarrow |3\rangle$  and the  $|3\rangle \leftrightarrow |4\rangle$  transitions (which are the transitions between the triplet states) will gradually attain the same value, namely the average  $\frac{\omega_0}{2}$  of the Larmor frequencies whereas the energies of the two transitions involving the singlet state  $|2\rangle$  will become proportional to  $J$ . In the case of strong coupling ( $\frac{J}{\hbar} \gg \Delta\omega$ ), the transition strength into the singlet states will eventually vanish which is why ESR spectroscopy of strongly coupled pairs typically is triplet spectroscopy. Since we are concerned with spin-dependent transport and recombination rates due to the spin-motion of ensembles of spin pairs, we use in analogy to the approach of Refs.<sup>9,10,11,13</sup> a density operator  $\hat{\rho} = \hat{\rho}(t)$  to represent the ensemble state. In the case of negligible incoherence which means on time scales faster than the electronic transition times and spin relaxation times, the dynamics of the ensemble is described by the Liouville equation  $\partial_t \hat{\rho} = \frac{i}{\hbar} [\hat{\rho}, \hat{H}]^-$ . When incoherence becomes non-negligible, the influence of spontaneous electronic transitions such as the recombination or dissociation of the electronic states as well as spin relaxation processes must be taken into account by means of statistical terms  $\mathcal{S}[\hat{\rho}]$  and  $\mathcal{R}[\hat{\rho} - \hat{\rho}_0]$ , respectively, as it has been described and outlined for Eq. 1 of Ref.<sup>13</sup>.

### A. PEDMR/pODMR observables

In contrast to observables of pESR signals which are always represented by polarization operators applied to a spin ensemble, the observables for spin-dependent transport and recombination rates are triplet and singlet operators<sup>13</sup>. The goal of this study is to make predictions for pEDMR/pODMR signals as they are observed in a transient nutation style experiment. Transient nutation can be observed electrically by application of a short coherent pulse with length  $\tau$  (typically a few nanoseconds) and the subsequent measurement of spin-dependent transport or recombination rates through transient measurement of the sample conductivity. When the applied radiation pulse changes the spin states of trapped charge carriers resonantly, spin-dependent transition rates change abruptly and then, after the pulse, they slowly (on microsecond to millisecond time scales) relax back into their steady states following an exponential rate transient

$$R(t) = \sum_{i=1}^4 \delta\rho_{ii}(\tau) r_i e^{-r_i t} \quad (2)$$

due to the spontaneous spin-dependent electronic transitions which collapse the coherently excited spin pairs<sup>12</sup>. In Eq. 2,  $\delta\rho_{ii}(\tau) = \rho_{ii}(\tau) - \rho_{ii}^S$  whereas  $\rho_{ii}(\tau)$  and  $\rho_{ii}^S$  denote the diagonal elements of the density matrices at the

end of the coherent excitation pulse  $\rho(\tau)$  and the steady state  $\rho^S$ , respectively. Both  $\rho(\tau)$  and  $\rho^S$  represent the density operator  $\hat{\rho}$  for the base of energy eigenstates. The variables  $r_i$  denote the spin-dependent recombination or transport rate coefficients of the spin states  $|i\rangle$  which in presence of exchange coupling attain the form

$$\begin{aligned} r_{1,4} &= r_T \\ r_{2,3} &= \frac{r_T}{2} \left[ 1 \mp \frac{J}{\hbar\omega_\Delta} \right] + \frac{r_S}{2} \left[ 1 \pm \frac{J}{\hbar\omega_\Delta} \right] \end{aligned} \quad (3)$$

with  $\omega_\Delta = \sqrt{J^2/\hbar^2 + \Delta\omega^2/4}$  and  $r_T$  and  $r_S$  denoting transition probabilities of pairs in pure triplet and pure singlet states, respectively<sup>13</sup>. Note that Eq. 2 derives from Eq. 17 of Ref.<sup>13</sup> for the case of spin-dependent recombination and Eq. 5.17 of Ref.<sup>12</sup> for the case of spin-dependent transport under the assumptions that all spin relaxation processes as well as spin-independent pair dissociation processes are much slower than the four spin-dependent transitions ( $r_i \gg d, T_1^{-1}, T_2^{-1}$ ). Because of these assumptions, the relaxation transient of each diagonal element  $\delta\rho_{ii}$  towards the steady state becomes a single exponential decay with decay constant  $r_i$ .

Similar to the integration of a free induction decay in a pESR experiment, the integration of the rate relaxation transient in a pODMR/pEDMR experiment

$$Q(\tau) := \int_0^{\tau} R(t) dt = \sum_{i=1}^4 \delta\rho_{ii}(\tau) (1 - e^{-r_i \tau}) \quad (4)$$

contains information about the state of the pair ensemble at  $t = 0$  which is the moment when the rate relaxation begins at the end of the excitation pulse with length  $\tau$ . Note that since  $Q(\tau)$  is the time integration of a rate, it is a dimension free variable representing a number of transitions that take place due to the pulse excitation. For a pODMR measurement this number translates directly into a photon number. For pEDMR where a current transient is integrated into a charge,  $Q(\tau)$  represents a number of elementary charges  $e$ . The assumption that coherence is preserved during the excitation pulse implies that  $\text{Tr}(\hat{\rho}(\tau)) = \text{Tr}(\hat{\rho}^S)$  and, therefore, if we integrate over large time scales ( $t_0 \rightarrow \infty$ ),  $Q(\tau)$  will vanish. This result is reasonable since we implicitly have assumed for our system that the generation rate of the spin pairs is constant and not changed by the pulse excitation. Hence, no matter what time dependence  $R(t)$  follows, averaged over a long time it must assume the generation rate of intermediate spin pairs. Note that the assumption of a constant spin pair generation rate is reasonable as long as the spin-dependent processes change the overall transport or recombination rates only slightly (less than  $10^{-2}$  as it is the case for most known pEDMR/pODMR signals) since then, generation rate changes will be negligible second order effects<sup>12</sup>. Hence, experimentally,  $Q(\tau)$  must be recorded for a finite value of the integration time  $t_0$ . Typically it is recorded for  $r_{2,3}^{-1} \ll t_0 \ll r_{1,4}^{-1} = r_T^{-1}$  since then, Eq. 4 assumes the form  $Q(\tau) = \delta\rho_{22}(\tau) + \delta\rho_{33}(\tau)$ .

For the case of negligible spin–spin coupling within the pairs, the situation becomes particularly simple since then  $\delta\rho_{22} = \delta\rho_{33} = -\delta\rho_{11} = -\delta\rho_{44}$  due to the symmetry of the pair Hamiltonian and, therefore,  $Q(\tau) \propto \delta\rho_{11}$ <sup>11</sup>. In this situation one may even measure  $Q(\tau)$  by integration over the absolute value of the current change in order to optimize signal strength as indicated in Fig. 5.7 of Ref.<sup>12</sup>. In contrast, with increasing exchange  $J$ ,  $\delta\rho_{22} \neq \delta\rho_{33}$  and as  $J$  becomes very large,  $r_2$  approaches  $r_T$  which means that there will be no well defined  $t_0$  which fulfills  $r_{1,4}^{-1} \gg t_0 \gg r_{2,3}^{-1}$ . One solution for this problem is to set  $t_0$  such that  $r_{1,3,4}^{-1} \gg t_0 \gg r_2^{-1}$  in order to observe transitions into singlet states only. However, with increasing  $J$  the singlet transition probability diminishes quickly and along with it any measurable signal. Alternatively, one can set  $t_0$  to an arbitrary but well defined value such as  $t_0 := 4r_3^{-1}$ . This ensures that all contributions from the singlet transitions and almost all ( $1 - e^{-4} \approx 98\%$ ) contributions of the triplet signal are recorded even though both signals will vanish at large  $J$  as well. For the simulations presented in the following we used the latter assumption ( $t_0 := 4r_3^{-1}$ ) for the calculation of the pEDMR/pODMR observable given in Eq. 4 in order to investigate both, the influences of singlet and triplet transitions on pEDMR/pODMR measurements and also, in order to elucidate how the magnitude of the two signals evolve relatively to each other as both become smaller with increasing  $J$ .

spin-dependent electronic transitions. The time domain signal  $Q(\tau)$  was calculated for pulse length  $0 \leq \tau \leq 1.5\mu\text{s}$  with a resolution of 1000 steps per nanosecond. These transients were then Fourier transformed in order to reveal the frequency components  $FT\{Q(\Omega)\}$ . In order to test the qualitative correctness of these results, an independent calculation of the nutation frequencies of the Hamiltonian  $\hat{H} = \hat{H}_0 + \hat{H}_J + \hat{H}_1(t)$  was conducted for each used set of parameters and compared to the results obtained numerically. In these test calculations the time evolution of the spin ensemble was studied by simply applying the time evolution operator  $\exp\left(-\frac{i\hat{H}^*\tau}{\hbar}\right)$  (with  $\hat{H}^*$  representing the time independent Hamiltonian of the pair in a reference frame that rotates with the circularly polarized magnetic field of the exciting radiation) to the reference frame independent initial state defined in Ref<sup>11</sup>. The test confirmed our numerical results. In Fig.2(a) to (i) the results of the numerical solutions of the stochastic Liouville equation (Eq. 5) are presented. They display the intensity of the pEDMR/pODMR signal as a function of their frequency components  $\Omega$  and the frequency  $\omega$  of the applied driving field. Note that these frequencies are expressed in terms of the field strength  $\gamma B_1$  of the driving field. The parameters used for the calculation of the data displayed in Fig. 2 represent the case of  $B_1 \ll B_0$  and thus  $\Omega \ll \omega$  as found in most pESR experiments. In fact the parameters used here represent typical values that can be established in modern, commercially available pESR X-Band

### III. CALCULATIONS AND RESULTS

The behavior of the observable  $Q(\tau)$  and its dependence on the exchange coupling parameter  $J$ , the frequency  $\omega$  and the amplitude  $B_1$  of the exciting radiation, Larmor frequency of the pair partners  $\omega_a$  and  $\omega_b$ , dissociation rate coefficient  $d$ , singlet and triplet recombination rates  $r_S$  and  $r_T$  and the generation rate  $G$  have been studied. As the field strength  $B_1$  is the parameter that is compared to the system parameter  $\Delta\omega$ , we consider three cases for the strength of the interaction between the  $B_1$ -field and the system, namely (i) high power  $\gamma B_1/\Delta\omega \gg 1$ , (ii) intermediate power  $\gamma B_1/\Delta\omega \approx 1$  and (iii) low power  $\gamma B_1/\Delta\omega \ll 1$  excitation with  $\gamma$  denoting the gyromagnetic ratio. Each of these cases is then simulated for (a) weak ( $\Delta\omega \gg \frac{J}{\hbar}$ ), (b) intermediate ( $\Delta\omega \approx \frac{J}{\hbar}$ ), and (c) strong ( $\Delta\omega \ll \frac{J}{\hbar}$ ) exchange coupling. The evolution of  $Q(\tau)$  with increasing pulse length  $\tau$  was calculated by numerical solutions of a systems of 16 partial differential equations which result from the statistical Liouville equation

$$\partial_t \hat{\rho} = \frac{i}{\hbar} [\hat{\rho}, H]^- + \mathcal{S}[\hat{\rho}] + \mathcal{R}[\hat{\rho} - \hat{\rho}_0] \quad (5)$$

in which the spin relaxation processes  $\mathcal{R}[\hat{\rho} - \hat{\rho}_0] \approx 0$  were neglected but not the incoherence  $\mathcal{S}[\hat{\rho}] \neq 0$  induced by the

spectrometers: For all data sets  $\omega' = \frac{\omega_a + \omega_b}{2} = 10\text{GHz}$ ,  $\frac{\gamma}{2\pi} B_1 = 10\text{MHz}$  and  $\frac{\omega_0}{2\pi} = 10\text{GHz}$ . Furthermore, for all simulations we assumed that the signal was caused by a spin-dependent electronic transition based on the intermediate pair model described above whose intermediate pairs had a singlet recombination rate coefficient  $r_S = 10^6\text{s}^{-1}$ , a triplet recombination rate coefficient  $r_T = 10^4\text{s}^{-1}$ , and a pair dissociation rate coefficient  $d = 10^3\text{s}^{-1}$  that is much smaller than the recombination probabilities. Note that the orders of magnitude of these values correspond to experimental data obtained from spin-dependent recombination processes at defects in different silicon morphologies<sup>5</sup>. The generation rate of the simulated pair ensemble was chosen arbitrary since it only scales the intensity of the calculated observable. However note that this arbitrary value was kept constant for all simulations presented here in order to make the signal intensities as plotted in Fig. 2 comparable. The data sets displayed in Fig. 2 represent the combination of three different Larmor separations ( $\Delta\omega=1, 20$ , and  $40\text{MHz}$ ) and three different exchange coupling constants ( $J/\hbar=1, 10$  and  $50\text{MHz}$ ). The choice of these values was made in order to establish the qualitative behavior of the system when  $\Delta\omega, J/\hbar \ll \gamma B_1$ ,  $\Delta\omega \ll \gamma B_1 \ll J/\hbar$ ,  $J/\hbar \ll \gamma B_1 \ll \Delta\omega$  and  $\gamma B_1 \ll \Delta\omega, J/\hbar$  as well as the intermediate cases where two or all three of these three parameters have comparable magnitudes. Note that for all cases it is assumed that  $J/\hbar, \Delta\omega, \gamma B_1 \ll \omega_a, \omega_b$  which implies that the results presented here will not be applicable to very strongly coupled excitonic states ( $J/\hbar \gg \omega_a, \omega_b$ )

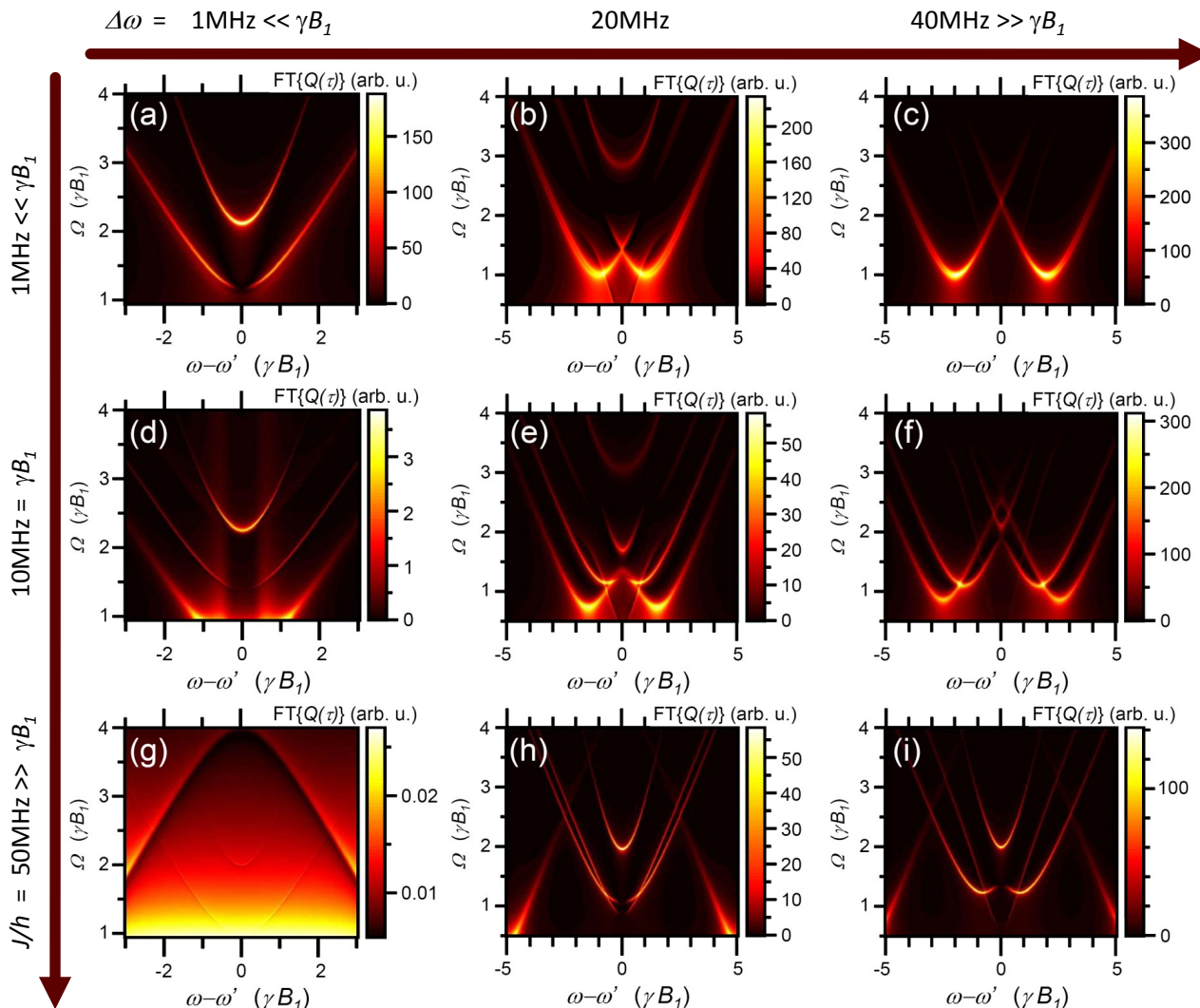


FIG. 2: Plots of the Fourier transform  $\text{FT}\{Q(\tau)\}$  of the observable  $Q(\tau)$ . The data displays the Fourier components of  $Q(\tau)$  as a function of the excitation (driving) frequency,  $\omega$ . Data sets are represented in arbitrary but equal units. They were simulated with Larmor separations of  $\Delta\omega = 1\text{MHz}$  (plots (a),(d),(g), left column),  $\Delta\omega = 20\text{MHz}$  (plots (b),(e),(h), center column) and  $\Delta\omega = 40\text{MHz}$  (plots (c),(f),(i), right column) as well as exchange coupling strengths with in the pairs of  $J/h = 1\text{MHz}$  (plots (a),(b),(c), first row),  $J/h = 10\text{MHz}$  (plots (d),(e),(f), second row) and  $J/h = 50\text{MHz}$  (plots (g),(h),(i), third row).

that can be found in many polymers and also in quantum dots. Note however that we will find in the following for cases of strongly yet not very strongly coupled pairs ( $\omega_a, \omega_b \gg J/\hbar \gg \Delta\omega$ ) that pEDMR and pODMR signals will vanish and hence, the consideration of very strongly coupled systems is not relevant in this case.

#### IV. DISCUSSION

The simulated data displayed in figs. 2(a-f) shows different hyperbola shaped structures which are known and expected for a resonant system with different eigenfrequencies. The symmetry centers of these structures represent the transition frequencies  $\omega_i$  which correspond

for all displayed data sets (and their corresponding parameter sets) to the energy differences that can be derived from Eq.1. Similarly as for the weakly exchange-coupled case described in Ref.<sup>11</sup>, the hyperbola shapes are caused by the increase of the transient nutation frequencies as the excitation frequency is detuned from a given resonance as described by Rabi's formula  $\Omega_i = \sqrt{(\gamma B_1)^2 + (\omega_i - \omega)^2}$ . In contrast to Ref.<sup>11</sup>, we see up to six different frequency components that exist for any given excitation frequency. The higher number of nutation components is anticipated since the introduction of the exchange Hamiltonian removed the symmetry from the four energy levels leading to four instead of just two transition energies (see Fig. 1 for the case of intermediate coupling  $J \approx \hbar\Delta\omega$ ) and correspondingly, to four

instead of two associated nutation frequencies. With two nutation frequencies given for the weakly exchange coupled case one can anticipate up to four different Rabi-frequency components when permutation symmetry and not polarization is detected with pEDMR and pODMR. Hence, the beat oscillations of the pair nutations can become dominating under certain conditions (for weakly coupled pairs this condition was  $\Delta\omega \ll \gamma B_1$ ). Therefore, with four nutation frequencies given for the strongly exchange coupled case one can anticipate an even larger number of Rabi-frequency components since as many as 12 combinations of these nutation frequencies are conceivable, even though not all of these may be dominant contributions. The presence of the beat oscillations can be verified from Fig. 2. The hyperbola shaped features around a resonance  $\omega_i$  turn into linear functions in their far off-resonant regions. The slopes of these linear functions are proportional to  $(\omega_i - \omega)$  for single nutation components. However, since beat oscillations resemble either the sum or the difference of single nutation components, their frequencies are either independent of  $\omega$  or proportional to  $2(\omega_i - \omega)$ . A comparison of the resonance hyperbolas in the different graphs of Fig. 2 shows that the beat oscillations are present whenever either  $\gamma B_1 \gg \Delta\omega$  (Fig. 2 a, d, g) or  $\frac{J}{\hbar} \gg \Delta\omega$  (Fig. 2 g, h, i) and in fact the only data set which did not indicate any beat component at all is shown in plot Fig. 2, c where  $\gamma B_1, \frac{J}{\hbar} \ll \Delta\omega$ . This confirms that when permutation symmetry is the observable (meaning for pEDMR or pODMR measurements) it is either the exchange coupling  $J$  or the interaction of both spins with the strong excitation fields  $\gamma B_1$  which determine whether the observed oscillations are due to nutations of the individual spin pair partners or the beat oscillations thereof.

The second insight gained from Fig. 2 is the magnitude of the nutation frequencies as well as their beat oscillations. For the pESR measurement of transient nutation it had been shown<sup>9</sup> that for large exchange coupling ( $\frac{J}{\hbar} \gg \Delta\omega, \gamma B_1$ ), the on-resonance nutation frequencies associated with the triplet transitions approach values of  $\Omega = \sqrt{2}\gamma B_1$  whereas the nutation frequencies associated with the singlet transitions (whose oscillator strengths sharply drop as  $J$  increases) approach  $\Omega = 0$ . In agreement with these predictions, we obtain for the nutation frequencies of the singlet transitions values that decrease from  $\Omega = \gamma B_1$  to  $\Omega = 0$  as  $J$  increases and for the nutation frequencies of the triplet transitions values that rise from  $\Omega = \gamma B_1$  as  $J$  increases. However, as  $J$  becomes very large, the triplet nutation frequencies become less and less dominant while beat oscillations become more dominant. As one can see from Fig. 2, these beat oscillations exhibit on-resonance frequencies of  $\Omega = 2\gamma B_1$  and not  $\Omega = 2\sqrt{2}\gamma B_1$  as one would anticipate from a simple addition of two frequencies. This behavior is consistent with the "nutation frequency doubling" described for the pEDMR/pODMR detection of weakly coupled pairs under strong  $B_1$  fields. However, it is in contrast to the observations with pESR of strongly exchanged coupled

spin pairs and at this time we are not aware of a straightforward picture that could provide a qualitative interpretation of this behavior.

The third observation that we obtain from the simulated data is that the ratio of the signal strengths of the observed singlet transitions and the triplet transitions does not change significantly as  $J$  is increased: In pESR spectroscopy of exchange coupled spin pairs, the strong decline of the oscillator strength of singlet transitions leads to a disappearance of the singlet signal in comparison to a triplet signal whose oscillator strength increases. In contrast, for pEDMR/pODMR experiments, the increase of  $J$  causes a drop-off of both the singlet and triplet signals. The singlet signal drops off for the same reasons as the singlet strength of pESR signals. In contrast, the triplet signal drops off since the transition from one triplet state into another triplet state does not change the permutation symmetry of the pairs and hence, a change of the detected electronic transition rate does not take place either. Note that the data sets presented in Fig. 2 are plotted with different color scales in order to display the data with optimal contrast. However, the arbitrary units to which the different color scales translate are equal for all nine displayed data sets. Thus, Fig. 2 illustrates how the signals drop as either the exchange coupling  $J$  or the Larmor separation  $\Delta\omega$  increases. The strongest decline of the signal intensity is in fact given in plot (g) where  $\Delta\omega$  is minimized and  $J$  is maximized. Note however that in spite of this decrease of the signal strengths, the relative strengths of the singlet and triplet contributions remain of comparable magnitude. Hence, as long as the sensitivity of a given pEDMR or pODMR experiment allows the detection of any signal under strong coupling, both the triplet and the singlet contributions should be equally well observable. This realization can be important for the verification of the nature of an observed spin pair system. It may be a way to distinguish experimentally the difference between a strongly exchange coupled system ( $\frac{J}{\hbar} \gg \Delta\omega$ ) and a weakly exchange coupled system where  $\frac{J}{\hbar} \ll \Delta\omega \ll \gamma B_1$ .

## V. SUMMARY AND CONCLUSIONS

The dynamics of spin-dependent electronic transport and recombination rates through strongly exchange-coupled spin pairs during coherent electron spin resonant excitation as it would be observed with pEDMR or pODMR detected transient nutation experiments has been simulated by numerical solution of the stochastic Liouville equation which accounted for incoherent effects. From the results we conclude that significant qualitative and quantitative differences can exist between pEDMR/pODMR experiments in comparison to pESR experiments conducted on the same systems. Similarly as for the weakly exchange coupled case, we observe that beat oscillations of the spin nutations and not the spin nutation alone dominate the transport or recombination

rates whenever either the exchange coupling strength  $J$  or the  $B_1$  field exceed the Larmor separation  $\Delta\omega$  within the pair. Moreover, while the intensities of the rate oscillations decrease with increasing exchange within the spin pairs, the singlet and triplet signals retain their relative strength. This means that pEDMR and pOMDR for both of which permutation symmetry is utilized as observable can provide insights and information about the nature of the observed spin systems which would hardly or not at all be accessible with conventional radiation (and, therefore, polarization-) detected electron spin resonance spectroscopy.

## Acknowledgments

A. G. gratefully acknowledges support by the Swiss National Foundation under Grant no. 200020-107428/1. C. M., S. D. B. and F. G. gratefully acknowledge Financial support of the Deutsche Forschungsgemeinschaft, of the Fonds der Chemischen Industrie, and the European Graduate College "Electron-Electron Interactions in Solids" Marburg-Budapest.

- 
- <sup>1</sup> C. B. Harris, R. L. Schlupp, and H. Schuch, *Phys. Rev. Lett.* **30**, 1019 (1973).
- <sup>2</sup> D. J. Gravesteijn and M. Glasbeek, *Phys. Rev. B* **19**, 5549 (1979).
- <sup>3</sup> E. van Oort and M. Glasbeek, in *Pulsed EPR a new field of application*, edited by C. P. Keijzers, E. J. Reijerse, and J. Schmidt (North Holland, Amsterdam, 1989), Chap. 19, pp. 227–231.
- <sup>4</sup> V. Weis, K. Möbius, and T. Prisner, *J. magn. Res.* **131**, 17 (1998).
- <sup>5</sup> C. Boehme and K. Lips, *Phys. Rev. Lett.* **91**, 246603 (2003).
- <sup>6</sup> J. R. Petta, A. C. Johnson, J. M. Taylor, E. A. Laird, A. Yacoby, M. D. Lukin, C. M. Marcus, M. P. Hanson, and A. C. Gossard, *Science* **309**, 2180 (2005).
- <sup>7</sup> T. Machida, T. Yamazaki, K. Ikushima, and S. Komiyama, *Appl. Phys. Lett.* **82**, 409 (2003).
- <sup>8</sup> F. H. L. Koppens, C. Buizert, K. J. Tielrooij, I. T. Vink, K. C. Nowack, T. Meunier, L. P. Kouwenhoven, and L. M. K. Vandersypen, *Nature* **442**, 766 (2006).
- <sup>9</sup> M. Gierer, A. van der Est, and D. Stehlik, *Chem. Phys. Lett.* **186**, 238 (1991).
- <sup>10</sup> S. Weber, G. Kothe, and J. R. Norris, *J. Chem. Phys.* **106**, 6248 (1997).
- <sup>11</sup> V. Rajevac, C. Boehme, C. Michel, A. Gliesche, K. Lips, S. D. Baranovskii, and P. Thomas, *Phys. Rev. B* **74**, 245206 (2006).
- <sup>12</sup> C. Boehme and K. Lips, in *Charge Transport in Disordered Solids with Applications in Electronics*, edited by S. Baranovski (John Wiley and Sons, Ltd., Chichester, England, 2006), Chap. 5, pp. 179–219.
- <sup>13</sup> C. Boehme and K. Lips, *Phys. Rev. B* **68**, 245105 (2003).